

Mutual Consistency Learning for Semi-supervised Medical Image Segmentation

Yicheng Wu^{a,*}, Zongyuan Ge^{b,c}, Donghao Zhang^c, Minfeng Xu^d, Lei Zhang^d,
Yong Xia^e, Jianfei Cai^a

^a*Department of Data Science & AI, Faculty of Information Technology,
Monash University, Melbourne, VIC 3800, Australia*

^b*Monash-Airdoc Research, Monash University, Melbourne, VIC 3800, Australia*

^c*Monash Medical AI, Monash eResearch Centre, Melbourne, VIC 3800, Australia*

^d*DAMO Academy, Alibaba Group, Hangzhou, 311121, China*

^e*School of Computer Science and Engineering, Northwestern Polytechnical University,
Xi'an 710072, China*

Abstract

In this paper, we propose a novel mutual consistency network (MC-Net+) to effectively exploit the unlabeled data for semi-supervised medical image segmentation. The MC-Net+ model is motivated by the observation that deep models trained with limited annotations are prone to output highly uncertain and easily mis-classified predictions in ambiguous regions (*e.g.*, adhesive edges or thin branches) for medical image segmentation. Leveraging these region-level challenging samples can make the semi-supervised segmentation model training more effective. Therefore, our proposed MC-Net+ model consists of two new designs. First, the model contains one shared encoder and multiple slightly different decoders (*i.e.*, using different up-sampling strategies). The statistical discrepancy of multiple decoders' outputs is computed to denote the model's uncertainty, which indicates the unlabeled hard regions. Second, we apply a novel mutual consistency constraint between one decoder's probability output and other decoders' soft pseudo labels. In this way, we minimize the discrepancy of multiple outputs (*i.e.*, the model uncertainty) during training and force the model to generate invariant results in such challenging regions, aiming at

*Corresponding Author

Email address: yicheng.wu@monash.edu (Yicheng Wu)

capturing more useful features. We compared the segmentation results of our MC-Net+ with five state-of-the-art semi-supervised approaches on three public medical datasets. Extension experiments with two common semi-supervised settings demonstrate the superior performance of our model over other existing methods, which sets a new state of the art for semi-supervised medical image segmentation. Our code will be released publicly¹.

Keywords: Mutual consistency, soft pseudo label, semi-supervised learning, medical image segmentation

1. Introduction

Medical image segmentation is a fundamental and critical step to construct a computer-aided diagnosis (CAD) system. Based on the accurate segmentation results, the morphological attributes of organs can be quantitatively analysed to provide useful basis for clinicians to diagnose diseases. At the same time, with an effective segmentation model, the localization of ROIs is significant for the early screening and risk assessment of relevant diseases (Masood et al., 2015).

Recent years have witnessed the remarkable progress of deep methods in medical image segmentation. However, they still suffer from sub-optimal performance on many medical tasks. Their limited performance is mainly attributed to the over-fitting caused by the inadequate training data, as most of medical image segmentation datasets are of small scale. This is because acquiring enough densely annotated medical data is extremely expensive. Manually annotating medical images (*e.g.*, volumetric CT or MRI scans) at the pixel/voxel-level not only requires expertise and concentration but also is time-consuming. Therefore, exploiting unlabeled medical data like semi-supervised approaches has become extremely important to improve the performance of medical image segmentation models and has attracted increasing research attention.

Existing semi-supervised methods can be roughly divided to two categories.

¹<https://github.com/ycwu1997/MC-Net>

The first approaches are the consistency-based models (Yu et al., 2019; Luo et al., 2021a,b) according to the smoothness assumption *i.e.*, *small perturbations of an input should not produce the obvious deviations of corresponding outputs* (Laine and Aila, 2016). The second category consists of several entropy-minimization methods (Lee et al., 2013; Rizve et al., 2021; Pham et al., 2021), which are based on the low-entropy assumption *i.e.*, *the cluster of each class should be compact and thus of low entropy*. However, most of existing methods do not make full use of the learning difficulties (Soviany et al., 2021) of unlabeled data in semi-supervised image segmentation tasks. Considering deep models can generate the segmentation results with the pixel/voxel- level uncertainties, we suggest to leverage such uncertainties to effectively exploit the unlabeled data, aiming at further improving the semi-supervised medical image segmentation performance.

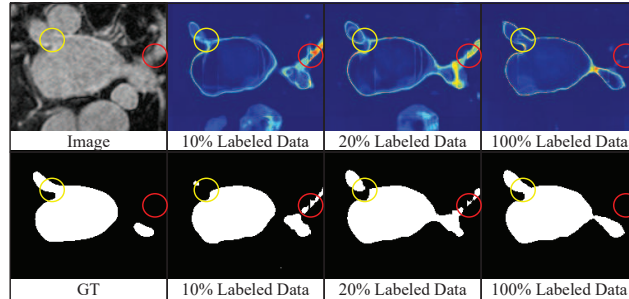


Figure 1: Three exemplar uncertainty maps and the corresponding segmented results of the fully supervised V-Net model, trained with 10%, 20% and all labeled data on the LA dataset.

Instead of following the curriculum learning (Soviany et al., 2021), our main idea is to exploit the learning for the unlabeled challenging regions to facilitate the model training. We further use Fig. 1 as an example to illustrate our motivation. Specifically, Fig. 1 gives three uncertainty maps and the segmentation results on the left artium (LA) dataset, which are obtained by three fully-supervised V-Net models, trained by 10%, 20% and all labeled data respectively. Each uncertainty map was obtained by the Monto-Carlo Dropout (MC-Dropout) method as (Yu et al., 2019). Fig. 1 indicates two key observa-

tions: (1) *The highly uncertain predictions mainly locate on some challenging regions (e.g., thin branch joints, indicated by the yellow and red circles in Fig. 1).* Meanwhile, the regions without complicated textures and varied appearances are more likely to be correctly segmented. In other words, trained with more labeled data, the V-Net model only refines the predictions of few hard areas; (2) *With the increase of labeled data for training, the model is prone to output less ambiguous results.* Thus, we hypothesize that the generalization ability of deep models should be highly related to the model uncertainty. These observations motivate us to explore the model uncertainty to help the model generalize to these hard regions, which also aligns with a concurrent work in (Qiao and Peng, 2021).

Therefore, in this paper, we propose a novel mutual consistency (MC-Net+) network for semi-supervised medical image segmentation, aiming to pay more attention to unlabeled challenging regions via the model uncertainty. First, as Fig. 2 shows, our MC-Net+ model is composed of one shared encoder and multiple slightly different decoders. The statistical discrepancy of multiple decoders’ outputs is used to represent the pixel/voxel- level uncertainty, indicating the hard regions. Second, we utilize a sharpening function to convert the probability outputs into soft pseudo labels. Then, we design a new mutual consistency training scheme, which enforces a consistency constraint between one decoder’s probability output and other decoders’ soft pseudo labels. In this way, we minimize the output discrepancy of multiple decoders during the model training and establish an ‘end-to-end’ way to train our model, attempting to capture more useful features from the unlabeled challenging regions.

Overall, our contributions of this paper are three-fold.

- We proposed the MC-Net+ model for semi-supervised segmentation, with the key idea that enforcing the model to generate consistent and low-entropy predictions in the hard regions can effectively exploit the unlabeled data and improve the semi-supervised image segmentation performance.
- We designed a novel mutual consistency scheme to take advantage of the

consistency and low-entropy constraints for the model training, enabling the model to learn a generalized feature representation.

- Extensive experiments demonstrate that the proposed MC-Net+ model outperforms five recent methods and sets a new state of the art (SOTA) for semi-supervised medical image segmentation.

The preliminary version of this work appeared in MICCAI 2021 (Wu et al., 2021), which encourages the mutual consistency between two slightly different decoders. This paper substantially extends the conference version. The main extensions include: (1) embedding another decoder using a nearest interpolating operation into the original MC-Net model, which further increases the intra-model diversity; (2) conducting experiments on the extra Pancreas-CT and ACDC datasets to demonstrate the general effectiveness of our model on other semi-supervised medical image segmentation tasks; (3) implementing five recent approaches in the same environment and reporting the corresponding results for fair comparisons; (4) supplementing the hyper-parameter discussions; (5) adopting the original encoder-decoder architecture for testing, without introducing additional inference costs.

2. Related Work

2.1. Semi-supervised Learning

Semi-supervised learning (SSL) is widely studied in various computer vision tasks. For the consistency-based models, many data augmentation methods (Zhang et al., 2017; Xie et al., 2019) are used to generate different perturbed data. For example, Ouali et al. (2020) enforced several data augmentation operations to perturb the intermediate feature maps and constrained the model to output invariant segmentation maps. Wang et al. (2021b) utilized the semantic direction in the feature space to achieve semantic data augmentation and then applied consistency constraints for SSL. Sohn et al. (2020) employed the consistency of training samples under weak and strong perturbations to

facilitate the model training. Consistency at the model level is also discussed in the mean-teacher model via using an exponential moving average (EMA) operation (Tarvainen and Valpola, 2017). Meanwhile, the adversarial training (Miyato et al., 2018; Mittal et al., 2019) is used to enforce stronger consistency constraints to enhance the model learning.

Additionally, the entropy minimization-based models can also boost the semi-supervised learning. For instance, Kalluri et al. (2019) proposed an entropy module to enable the model to generate low-entropy predictions on the unlabeled dataset. Furthermore, the pseudo label learning (Lee et al., 2013; Chen et al., 2021) often employs a sharpening function or a fixed threshold to convert probability maps into pseudo labels. Then, supervised by pseudo labels, the model can learn to generate low-entropy results. For example, Rizve et al. (2021) unitized the probability and uncertainty thresholds to select the most accurate pseudo labels for SSL. Pham et al. (2021) incorporated the meta learning scheme into the pseudo label learning to improve performance.

It is nowadays widely recognized that both the consistency constraint and the low-entropy constraint can boost the feature discriminatory power of semi-supervised models. Therefore, in this paper, we employ both techniques in our MC-Net+ model for accurate semi-supervised medical image segmentation.

2.2. Semi-supervised Medical Image Segmentation

Several recent semi-supervised methods have been proposed for the medical image segmentation task. For example, Yu et al. (2019) proposed an uncertainty-aware mean-teacher model for semi-supervised left atrium segmentation. Li et al. (2020b) further enforced the shape constraints via introducing the signed distance map (SDM) (Ma et al., 2020) to improve the performance. Meanwhile, Luo et al. (2021a) studied the relation between medical image segmentation and organ shape regression. They also investigated a semi-supervised model to learn multi-scale consistency for the gross target volume segmentation (Luo et al., 2021b). Furthermore, Xia et al. (2020b,a) employed a multi-view co-training strategy to perform ensemble learning for 3D medical image segmentation.

Xie et al. (2020) utilized the attention mechanism to extract the pair-wise relation between labeled and unlabeled data to further relieve the over-fitting caused by limited labeled data.

Although these models have reported encouraging results for semi-supervised medical image segmentation, they still neglect or underestimate the effects of the unlabeled challenging regions during the model training. In other words, we hypothesize that the performance of our task can be further improved via more effective modeling the challenging regions even without corresponding labels. Note that, we noticed that the CPS model (Chen et al., 2021) recently developed a cycled-consistent model similar to ours for semi-supervised image segmentation, but their model employs an identical model architecture with different initialization parameters and enforces different input noises to perturb input images. In contrast, our model is motivated by Fig. 1 and adopts a shared encoder with multiple slightly different decoders for training. Section 6.1 further demonstrates that using different up-sampling strategies can lead to better segmentation results.

2.3. Multi-task Learning

Another research direction to improve the generalization of a deep learning model is through learning a cross-task feature representation or multi-task learning. For example, the contrastive learning-based models (Chaitanya et al., 2020) leverage the self-supervised training to mitigate the over-fitting of deep models (You et al., 2021b,a; Wu et al., 2022). Furthermore, some proxy or auxiliary tasks can be constructed to explicitly regularize the image segmentation (Zhu et al., 2020). For instance, the shape or boundary constrains (Li et al., 2020b; Luo et al., 2021a; Ma et al., 2020; Murugesan et al., 2019) are able to refine the shapes of segmentation results. Auxiliary losses (Wang et al., 2021a; Castillo-Navarro et al., 2020) (*e.g.*, for the image reconstruction task) can also help the model extract more generalized features.

Compared to these successful methods, our proposed MC-Net+ model does not need to design specific auxiliary tasks and only considers the original seg-

mentation task for the model training. On the other hand, our proposed method can be easily incorporated with those multi-task learning models to further boost the semi-supervised image segmentation performance.

2.4. Uncertainty Estimation

The uncertainty analysis attracts much attention in the both fields of machine learning and medical image processing (Abdar et al., 2021; Jungo and Reyes, 2019). We not only expect the model output correct results, but also expect to obtain the confidence of the results. For example, the inherent aleatoric uncertainty is caused by the annotation noises and the epistemic uncertainty accounts for the discrepancy of deep models (Kendall and Gal, 2017). In semi-supervised scenarios, we only discuss the epistemic uncertainty, which can be reduced by giving more training data.

There are some existing methods to estimate it. For example, Jin et al. (2019) employed the variational U-Net (Esser et al., 2018) to represent the model’s uncertainty. The epistemic uncertainty can be also quantified via the model ensemble strategy (Lakshminarayanan et al., 2016), which computes the statistical discrepancy of different outputs of several individually trained models. However, this scheme would bring more computational costs. To address this, in Bayesian modeling, the MC-Dropout method is proposed to approximate the model’s uncertainty in a flexible way (Gal and Ghahramani, 2016). Specifically, the dropout operation can sample multiple sub-models from the whole model. The statistical discrepancy of sub-models’ outputs can be used to compute the model’s uncertainty. In this way, there is no need to train multiple models individually. In this paper, inspired by (Zheng and Yang, 2021), our model pre-defined the sub-models before the model training, which can estimate the model’s epistemic uncertainty in only one forward pass.

3. Method

Before introducing our model, we first define the semi-supervised segmentation problem with a set of notations. We use $x \in X$ to denote an input

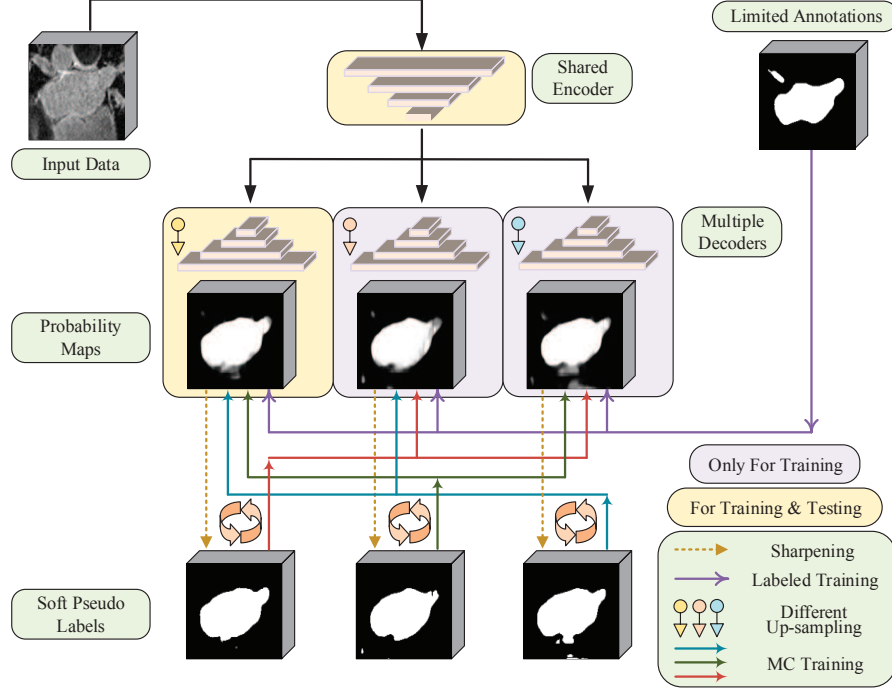


Figure 2: Diagram of our proposed MC-Net+ model, where the mutual consistency constraint is applied between one decoder’s probability output and the other decoders’ soft pseudo labels. Note that, in this paper, there are three slightly decoders in our MC-Net+ model.

image and $p(y_{pred}|x; \theta)$ is the probability map of the output prediction, where θ denotes the parameters of a deep model f_θ . Let $y_l \in Y_l$ denote the given segmentation annotations. The labeled and unlabeled sets are denoted as $\mathbb{D}_L = \{x_l^i, y_l^i | i = 1, \dots, N_l\}$ and $\mathbb{D}_U = \{x_u^i | i = 1, \dots, N_u\}$, respectively.

3.1. Model Architecture

The proposed MC-Net+ model attempts to exploit the unlabeled ambiguous regions for the model training, which can be indicated via the model’s epistemic uncertainty. Essentially, the normal uncertainty estimation process can be defined as follows:

$$\begin{aligned}
 f_{\theta_{sub}} &= Sampling(f_\theta) \\
 \mu_x &= D[p(y_{pred}|x; \theta_{sub}^1), \dots, p(y_{pred}|x; \theta_{sub}^n)]
 \end{aligned} \tag{1}$$

where D computes the statistical discrepancy of n outputs. μ_x is the pixel/voxel-level uncertainty of x . In MC-Dropout, the dropout operation samples n sub-models $f_{\theta_{sub}}$ from the whole model f_{θ} in n forward passes.

To address the issue that the MC-Dropout algorithm requires a lot of forward passes (more than eight times in (Yu et al., 2019; Rizve et al., 2021)), we design our model with one encoder and n slightly different decoders. Fig. 2 shows the architecture of our proposed MC-Net+ model. With a shared encoder f_{θ_e} , we pre-define n sub-models before the uncertainty estimation. Thus, the uncertainty μ_x of an input x becomes:

$$\begin{aligned} f_{\theta_{sub}^i} &= f_{\theta_e} \boxplus f_{\theta_d^i}, \quad i \in 1, \dots, n \\ \mu_x &= D[p(y_{pred}|x; \theta_{sub}^1), \dots, p(y_{pred}|x; \theta_{sub}^n)] \end{aligned} \quad (2)$$

where the symbol \boxplus means that a sub-model $f_{\theta_{sub}^i}$ is composed of one encoder f_{θ_e} and one decoder $f_{\theta_d^i}$. In other words, each sub-model $f_{\theta_{sub}^i}$ is the standard encoder-decoder architecture like V-Net or U-Net (Milletari et al., 2016; Ronneberger et al., 2015).

Specifically, to achieve a nice trade-off between effectiveness and efficiency, n is set as 3 in this paper (see Fig. 2). Here, we employ the transposed convolutional layer, the linear interpolation layer, and the nearest interpolation layer to construct three slightly different sub-models, aiming at increasing the intra-model diversity. In this way, we can approximate the model uncertainty more accurately to achieve better performance of semi-supervised medical image segmentation. These settings are further discussed in Section 6.2.

3.2. Training via Mutual Consistency Constraints

Based on such a model design, the discrepancy of multiple model outputs can be used to represent the model’s uncertainty, which indicates the challenging regions. Then, considering that both the consistency and the low-entropy constraints can help the model exploit the unlabeled data, we design a novel mutual consistency training strategy, applying two aforementioned constraints to effectively explore unlabeled challenging regions to train our model.

Specifically, using a sharpening function (Xie et al., 2019), we first convert an output probability map $p(y_{pred}|x; \theta)$ into a soft pseudo label $p^*(y_{pred}^*|x; \theta)$ defined as:

$$p^*(y_{pred}^*|x; \theta) = \frac{p(y_{pred}|x; \theta)^{1/T}}{p(y_{pred}|x; \theta)^{1/T} + (1 - p(y_{pred}|x; \theta))^{1/T}} \quad (3)$$

where T is a hyper-parameter to control the temperature of sharpening. Appropriate T not only can enforce the entropy minimization to regularize our model, but also would not bring much noises to confuse the model learning. We refer the readers to Section 6.3 for more details.

Then, we perform the mutual learning (Zhang et al., 2018) between one decoder’s probability output and other decoders’ soft pseudo labels. In this way, the discrepancy of n outputs is reduced to guide the model training and the predictions in these highly uncertain regions should be similar. The advantages of such a design can be concluded as: (1) the consistency constraints are enforced via encouraging the invariant outputs of all sub-models; (2) under the supervision of soft pseudo labels, the model is learned to generate low-entropy results as entropy minimization constraints; (3) the MC-Net+ model can be trained in an ‘end-to-end’ manner without multiple forward passes.

Finally, we employ the weighted sum of a supervised loss and a mutual consistency loss to train our proposed MC-Net+ model as the following:

$$L_{mc} = \sum_{i,j=1 \text{ \& } i \neq j}^n D[p^*(y_{pred}^*|x; \theta_{sub}^i), p(y_{pred}|x; \theta_{sub}^j)] \quad (4)$$

$$Loss = \lambda \times \sum_{i=1}^n L_{seg}(p(y_{pred}|x; \theta_{sub}^i), y_l) + \beta \times L_{mc} \quad (5)$$

where L_{seg} is the popular Dice loss for the segmentation task, and D is the Mean Squared Error (MSE) loss with paired inputs, *i.e.*, $p^*(y_{pred}^*|x; \theta_{sub}^i)$ and $p(y_{pred}|x; \theta_{sub}^j)$. λ and β are two hyper-parameters to balance the supervised loss L_{seg} and the mutual consistency loss L_{mc} . Note that, the L_{mc} is applied on both labeled and unlabeled sets \mathbb{D}_L and \mathbb{D}_U .

4. Experiment

4.1. Datasets

We evaluated the proposed MC-Net+ model on the LA, Pancreas-CT and ACDC datasets. The LA dataset (Xiong et al., 2021), the bench-marking dataset for the 2018 Atrial Segmentation Challenge², contains 100 gadolinium-enhanced MR imaging scans for training, with an isotropic resolution of $0.625 \times 0.625 \times 0.625$ mm. Since the testing set on LA does not include public annotations, followed by existing models (Yu et al., 2019; Li et al., 2020b; Luo et al., 2021a), we applied a fixed split³ of 80 samples for training and 20 samples for validation. Then, we report the performance of our model and other methods on the same validation set for fair comparisons.

The Pancreas-CT dataset (Clark et al., 2013) contains 82 3D abdominal contrast enhanced CT scans, which are collected from 53 male and 27 female subjects at the National Institutes of Health Clinical Center⁴. These slices are collected on Philips and Siemens MDCT scanners and have a fixed resolution of 512×512 with varying thickness from 1.5 to 2.5 mm. The data split is fixed in this paper as the DTC model (Luo et al., 2021a). We employed 62 samples for training and report the performance on the rest 20 samples. We then clipped the voxel values to the range of $[-125, 275]$ hounsfield units (HU) as (Zhou et al., 2019) and further re-sampled the data into an isotropic resolution of $1.0 \times 1.0 \times 1.0$ mm.

The ACDC (Automated Cardiac Diagnosis Challenge) dataset was collected from real clinical exams acquired at the University Hospital of Dijon⁵ (Bernard et al., 2018). The ACDC dataset contains cardiac MR imaging samples (multi-slice 2-D cine MRI) from 100 patients for training and 50 patients for testing. Also, following (Luo, 2020), we used a fixed data split⁶ in the patient level for our

²<http://atriaseg2018.cardiacatlas.org>

³<https://github.com/yulequan/UA-MT/tree/master/data>

⁴<https://wiki.cancerimagingarchive.net/display/Public/Pancreas-CT>

⁵<https://www.creatis.insa-lyon.fr/Challenge/acdc/databases.html>

⁶<https://github.com/HiLab-git/SSL4MIS/tree/master/data/ACDC>

experiments, where the new training, validation and testing sets respectively contain 70, 10 and 20 patients’ data. Unlike the task is 3D binary segmentation on the LA and Pancreas-CT datasets, we extend our model to the 2D multi-class segmentation task on the ACDC dataset. The 2D MC-Net+ model is designed to segment three targets including the myocardium, left and right ventricles from the 2D MR slices.

4.2. Implementing Details

3D Segmentation: Following (Yu et al., 2019; Li et al., 2020b; Luo et al., 2021a), we first cropped the 3D samples according to the ground truth, with enlarged margins *i.e.* $[10 \sim 20, 10 \sim 20, 5 \sim 10]$ or $[25, 25, 25]$ voxels on LA or Pancreas-CT, respectively. Then, these scans were normalized as zero mean and unit variance. For training, we randomly extracted 3D patches of size $112 \times 112 \times 80$ on LA or $96 \times 96 \times 96$ on Pancreas-CT.

Afterwards, we applied the 2D rotation and flip operations to the LA dataset for data augmentation. Then, on both datasets, the batch size was set as 4 and each batch contained two labeled patches and two unlabeled patches. The 3D backbone is V-Net, which uses the tri-linear interpolation layer to enlarge the feature maps. We trained our 3D MC-Net+ model for 15k iterations. For testing, we employed a sliding window of size $112 \times 112 \times 80$ or $96 \times 96 \times 96$ with a fixed stride $18 \times 18 \times 4$ or $16 \times 16 \times 16$ to extract patches on LA or Pancreas-CT, respectively. Then, we recomposed the patch-based predictions as final entire results.

2D Segmentation: On the ACDC dataset, we also normalized the samples as zero mean and unit variance. The random rotation and flip operations were applied as data augmentation. The 2D patches of size 256×256 were randomly extracted and the batch size was set as 24. Each batch included 12 labeled data and 12 unlabeled samples. In the testing time, we resized the scans to 256×256 as input and then enlarged it to the original size as final results. Our 2D MC-Net+ adopts the U-Net model as the backbone, which utilizes the bi-linear interpolation to expand the feature maps. The 2D model was trained

via 30k iterations. All settings on the ACDC dataset were followed the public benchmark (Luo, 2020) for fair comparisons.

On all datasets, we adopt the SGD optimizer with a learning rate 10^{-2} and a weight decay factor 10^{-4} for training. T or λ was respectively set as 0.1 or 0.5. The weight β was set as a time-dependent Gaussian warming-up function (Laine and Aila, 2016) as public methods (Yu et al., 2019; Li et al., 2020b; Luo et al., 2021a; Wu et al., 2021), which can mitigate the impacts of inaccurate mutual consistency loss during the early training stage. Note that, we performed two typical semi-supervised experimental settings *i.e.*, training with 10% or 20% labeled data and the rest unlabeled data, as (Yu et al., 2019; Li et al., 2020b; Luo et al., 2021a). In this paper, we re-implemented all compared methods and conducted the experiments in the identical environment (Hardware: Intel(R) Xeon(R) Gold 6150 CPU@2.70GHz, NVIDIA Tesla V100 GPU; Software: PyTorch 1.8.0, CUDA 11.2 and Python 3.8.10; Random Seed: 1337). Following (Yu et al., 2019; Li et al., 2020b; Luo et al., 2021a; Wu et al., 2021), we adopt four metrics including Dice, Jaccard, the average surface distance (ASD) and the 95% Hausdorff Distance (95HD) for the quantitative evaluation.

5. Result

5.1. Performance on the LA Dataset

Fig. 3 gives several segmentation results from two samples in 2D and 3D views on the LA dataset. They are obtained by five recent models and our method from left to right. It can be seen that the MC-Net+ model generates more complete left atrium than other SOTA methods. Note that, we do not use any morphological operations to refine the segmented results *e.g.* selecting the largest connected component as the post-processing module (Li et al., 2020b). Our model naturally eliminates most of isolated regions and preserves more fine details (indicated by purple and yellow arrows in Fig. 3) for the semi-supervised left atrium segmentation.

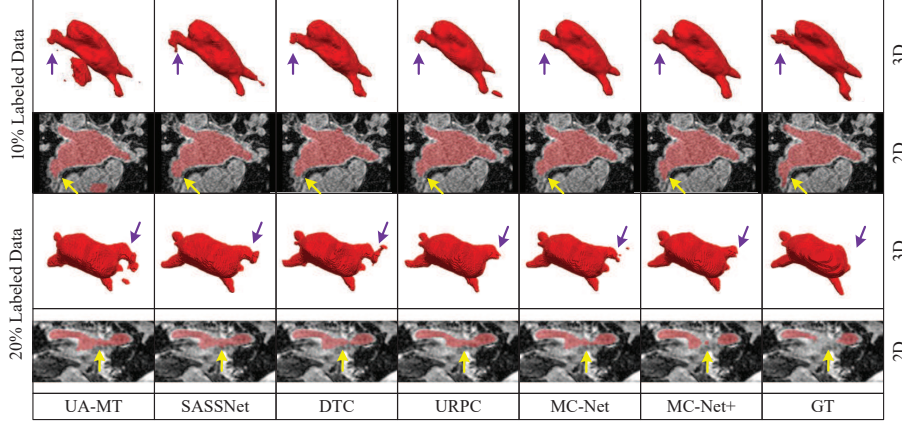


Figure 3: From left to right, there are several exemplar results in 2D and 3D views obtained by the UA-MT (Yu et al., 2019), SASSNet (Li et al., 2020b), DTC (Luo et al., 2021a), URPC (Luo et al., 2021a), MC-Net (Wu et al., 2021), and our MC-Net+ model on the LA dataset, equipped with the corresponding ground truth (right).

Table 1: Comparisons with five state-of-the-art methods on the LA dataset. Note that, the model complexities, *i.e.*, the number of parameters (*Para.*) and multiply-accumulate operations (*MACs*), are measured during the model inference.

conda								
Method	# Scans used		Metrics				Complexity	
	Labeled	Unlabeled	Dice(%) \uparrow	Jaccard(%) \uparrow	95HD(voxel) \downarrow	ASD(voxel) \downarrow	Para.(M)	MACs(G)
V-Net	8(10%)	0	78.57	66.96	21.20	6.07	9.44	47.02
V-Net	16(20%)	0	86.96	77.31	11.85	3.22	9.44	47.02
V-Net	80(All)	0	91.62	84.60	5.40	1.64	9.44	47.02
UA-MT (Yu et al., 2019) (MICCAI)	8 (10%)	72 (90%)	86.28	76.11	18.71	4.63	9.44	47.02
SASSNet (Li et al., 2020b) (MICCAI)			85.22	75.09	11.18	2.89	9.44	47.05
DTC (Luo et al., 2021a) (AAAI)			87.51	78.17	8.23	2.36	9.44	47.05
URPC (Luo et al., 2021b) (MICCAI)			85.01	74.36	15.37	3.96	5.88	69.43
MC-Net (Wu et al., 2021) (MICCAI)			87.50	77.98	11.28	2.30	12.35	95.15
MC-Net+ (Ours)			88.96	80.25	7.93	1.86	9.44	47.02
UA-MT (Yu et al., 2019) (MICCAI)	16 (20%)	64 (80%)	88.74	79.94	8.39	2.32	9.44	47.02
SASSNet (Li et al., 2020b) (MICCAI)			89.16	80.60	8.95	2.26	9.44	47.05
DTC (Luo et al., 2021a) (AAAI)			89.52	81.22	7.07	1.96	9.44	47.05
URPC (Luo et al., 2021b) (MICCAI)			88.74	79.93	12.73	3.66	5.88	69.43
MC-Net (Wu et al., 2021) (MICCAI)			90.12	82.12	8.07	1.99	12.35	95.15
MC-Net+ (Ours)			91.07	83.67	5.84	1.67	9.44	47.02

Table 1 gives the quantitative results on the LA dataset. It also shows the results of fully supervised V-Net model with 10%, 20% and all labeled data as the reference. By effectively leveraging the unlabeled data, our proposed MC-Net+

achieves impressive performance gains from 55% to 70% of Dice with only 10% labeled training data. Meanwhile, the model with only 20% labeled training data obtains comparable results *e.g.*, 91.07% vs. 91.62% of Dice, comparing with the upper bound (V-Net with 100% labeled training data). At the same time, as depicted in Table 1, our MC-Net+ model significantly outperforms the other methods in two semi-supervised settings and does not introduce more inference costs compared to the V-Net backbone.

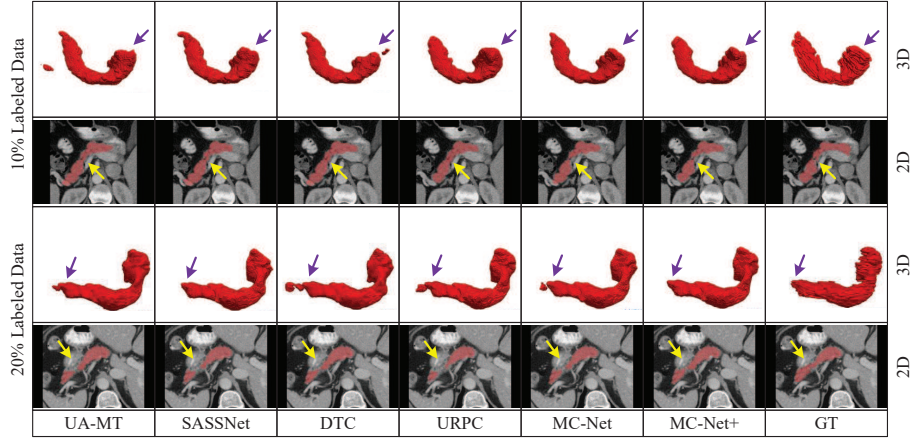


Figure 4: From left to right, there are several exemplar results in 2D and 3D views obtained by the UA-MT (Yu et al., 2019), SASSNet (Li et al., 2020b), DTC (Luo et al., 2021a), URPC (Luo et al., 2021a), MC-Net (Wu et al., 2021), and our MC-Net+ model on the Pancreas-CT dataset, equipped with the corresponding ground truth (right).

5.2. Performance on the Pancreas-CT Dataset

Fig. 4 and Table 2 show the corresponding results of our model and five semi-supervised methods on the Pancreas-CT dataset. Except for the multi-scale consistency method (Luo et al., 2021b), our proposed MC-Net+ model achieved the highest Dice and Jaccard than other methods for semi-supervised pancreas segmentation. Here, the original mutual consistency constraint is only performed at the single scale. However, the pancreas segmentation is a relatively difficult task and may require more multi-scale information. Therefore, based

Table 2: Comparisons with five state-of-the-art methods on the Pancreas-CT dataset. Note that, the model complexities, *i.e.*, *the number of parameters (Para.) and multiply-accumulate operations (MACs)*, are measured during the model inference.

Method	# Scans used		Metrics				Complexity	
	Labeled	Unlabeled	Dice(%) \uparrow	Jaccard(%) \uparrow	95HD(voxel) \downarrow	ASD(voxel) \downarrow	Para.(M)	MACs(G)
V-Net	6 (10%)	0	54.94	40.87	47.48	17.43	9.44	41.45
V-Net	12 (20%)	0	71.52	57.68	18.12	5.41	9.44	41.45
V-Net	62 (All)	0	82.60	70.81	5.61	1.33	9.44	41.45
UA-MT (Yu et al., 2019) (MICCAI)	6 (10%)	56 (90%)	66.44	52.02	17.04	3.03	9.44	41.45
SASSNet (Li et al., 2020b) (MICCAI)			68.97	54.29	18.83	1.96	9.44	41.48
DTC (Luo et al., 2021a) (AAAI)			66.58	51.79	15.46	4.16	9.44	41.48
URPC (Luo et al., 2021b) (MICCAI)			73.53	59.44	22.57	7.85	5.88	61.21
MC-Net (Wu et al., 2021) (MICCAI)			69.07	54.36	14.53	2.28	12.35	83.88
MC-Net+ (Ours)			70.00	55.66	16.03	3.87	9.44	41.45
<i>Multi-scale MC-Net+*</i>			74.01	60.02	12.59	<i>3.34</i>	5.88	61.21
UA-MT (Yu et al., 2019) (MICCAI)	12 (20%)	50 (80%)	76.10	62.62	10.84	2.43	9.44	41.45
SASSNet (Li et al., 2020b) (MICCAI)			76.39	63.17	11.06	1.42	9.44	41.48
DTC (Luo et al., 2021a) (AAAI)			76.27	62.82	8.70	2.20	9.44	41.48
URPC (Luo et al., 2021b) (MICCAI)			80.02	67.30	8.51	1.98	5.88	61.21
MC-Net (Wu et al., 2021) (MICCAI)			78.17	65.22	6.90	1.55	12.35	83.88
MC-Net+ (Ours)			79.37	66.83	8.52	1.72	9.44	41.45
<i>Multi-scale MC-Net+*</i>			80.59	68.08	6.47	<i>1.74</i>	5.88	61.21

* We designed our multi-scale MC-Net+ model based on (Luo et al., 2021b).

on (Luo et al., 2021b), we further design a new multi-scale MC-Net+ model, achieving the best performance in each setting on the Pancreas-CT dataset, see Table 2. It demonstrates that our proposed model can be easily incorporated with other multi-scale methods to further improve the segmentation performance. Moreover, our model does not rely on any post-processing modules and we do not use any shape-related constrains to train our model. Similar with the results of left atrium, our single-scale MC-Net+ model is able to obtain comparable performance in terms of the surface-based metrics and accurately segment the challenging areas, indicated by the purple and yellow arrows in Fig. 4, on the Pancreas-CT dataset.

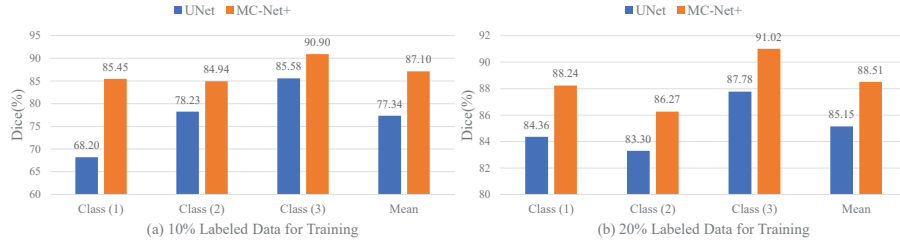
5.3. Performance on the ACDC Dataset

We further extend our model for the 2D multi-class segmentation task. The results in Table 3 are the average performance of three segmented targets *i.e.*, *the myocardium, left and right ventricles* on the ACDC dataset. It indicates that: (1) comparing with other methods, our model obtained the highest Dice, Jaccard

Table 3: Comparisons with five state-of-the-art methods on the ACDC dataset. Note that, the model complexities, *i.e.*, the number of parameters (*Para.*) and multiply-accumulate operations (*MACs*), are measured during the model inference.

Method	# Scans used		Metrics				Complexity	
	Labeled	Unlabeled	Dice(%) \uparrow	Jaccard(%) \uparrow	95HD(voxel) \downarrow	ASD(voxel) \downarrow	Para.(M)	MACs(G)
U-Net	7 (10%)	0	77.34	66.20	9.18	2.45	1.81	2.99
U-Net	14 (20%)	0	85.15	75.48	6.20	2.12	1.81	2.99
U-Net	70 (All)	0	91.65	84.93	1.89	0.56	1.81	2.99
UA-MT (Yu et al., 2019) (MICCAI)	7 (10%)	63 (90%)	81.58	70.48	12.35	3.62	1.81	2.99
SASSNet (Li et al., 2020b) (MICCAI)			84.14	74.09	5.03	1.40	1.81	3.02
DTC (Luo et al., 2021a) (AAAI)			82.71	72.14	11.31	2.99	1.81	3.02
URPC (Luo et al., 2021b) (MICCAI)			81.77	70.85	5.04	1.41	1.83	3.02
MC-Net (Wu et al., 2021) (MICCAI)			86.34	76.82	7.08	2.08	2.58	5.39
MC-Net+ (Ours)			87.10	78.06	6.68	2.00	1.81	2.99
UA-MT (Yu et al., 2019) (MICCAI)	14 (20%)	56 (80%)	85.87	76.78	5.06	1.54	1.81	2.99
SASSNet (Li et al., 2020b) (MICCAI)			87.04	78.13	7.84	2.15	1.81	3.02
DTC (Luo et al., 2021a) (AAAI)			86.28	77.03	6.14	2.11	1.81	3.02
URPC (Luo et al., 2021b) (MICCAI)			85.07	75.61	6.26	1.77	1.83	3.02
MC-Net (Wu et al., 2021) (MICCAI)			87.83	79.14	4.94	1.52	2.58	5.39
MC-Net+ (Ours)			88.51	80.19	5.35	1.54	1.81	2.99

and comparable surface-related performance in each semi-supervised setting; (2) via exploiting the unlabeled data effectively, our model almost produced the an average Dice gain of 10% or 3% than the fully-supervised U-Net model trained with 10% or 20% labeled data. Additionally, Fig. 5 shows the dice performance in each class, obtained by the fully-supervised UNet model and our semi-supervised MC-Net+ model. We can see that, either with 10% or 20% labeled data for training, our MC-Net+ model achieves impressive performance



5

Figure 5: Dice performance in each class on the ACDC dataset, obtained by the fully supervised UNet model and our semi-supervised MC-Net+ model, with 10% (a) and 20% (b) labeled data for training.

gains for the segmentation in each class.

Overall, based on the results on the three datasets, our MC-Net+ model shows superior performance than other SOTA methods for semi-supervised medical image segmentation. Note that, our model does not rely on specific backbones and can be applied for various medical tasks in either 2D or 3D segmentation. Meanwhile, it demonstrates that adding another decoder to increase the model’s diversity leads to the improved semi-supervised segmentation performance on all datasets (*i.e.*, MC-Net+ model vs. MC-Net model (Wu et al., 2021)).

Furthermore, we find three interesting properties of our proposed model: (1) the model without any shape-related constraints can generate satisfied segmented results with fewer isolated regions; (2) our MC-Net+ is effective to segment some challenging regions *e.g.*, thin branch joints in Fig. 3; (3) for testing, the MC-Net+ model does not introduce additional inference costs. These properties are beneficial for constructing an automatic CAD system to diagnose relevant diseases in practical clinical analysis.

6. Discussion

6.1. Ablation Study

The ablation studies (see Table 4) were conducted on the LA dataset, to show the effectiveness of each design. It reveals that, trained with 10% or 20% labeled data, (1) the most significant performance gains (*the average dice gains are 5.28% and 4.59%, respectively*) are achieved by forcing three decoders to generate similar results (*i.e.*, reducing the model uncertainty); (2) using multiple slightly different decoders, labeled by *DD*, results in average dice gains of 0.63% and 0.13%. Note that, a concurrent work (Chen et al., 2021) used identical model architectures with different initialization parameters while we employ different up-sampling strategies to further increase the intra-model diversity, leading to a better performance; (3) encouraging the mutual consistency for training, labeled by *MC*, is always better than applying consistency constraints

Table 4: Ablation studies of our MC-Net+ model on the LA dataset. Note that, *DD* means using different up-sampling strategies to construct three decoders, *CC* means only enforcing the consistency constraints for only $p(y_{pred}|x; \theta_{sub})$ or $p^*(y_{pred}^*|x; \theta_{sub})$, and *MC* means applying the mutual consistency constraints between $p(y_{pred}|x; \theta_{sub})$ and $p^*(y_{pred}^*|x; \theta_{sub})$.

# Scans used		Designs			Metrics			
Labeled	Unlabeled	<i>DD</i>	<i>CC</i>	<i>MC</i>	Dice(%) \uparrow	Jaccard(%) \uparrow	95HD(voxel) \downarrow	ASD(voxel) \downarrow
8 (10%)	0				82.69	70.93	28.27	7.89
8 (10%)	72 (90%)			✓	87.61	78.17	13.65	3.09
				✓*	88.33	79.31	9.17	1.92
				✓	88.58	79.68	7.79	2.01
		✓	✓		88.65	79.77	9.24	2.20
		✓	✓*		88.70	79.85	8.08	2.03
		✓		✓	88.96	80.25	7.93	1.86
16 (20%)	0				86.01	75.92	19.27	4.84
16 (20%)	64 (80%)			✓	90.60	82.90	7.44	2.28
				✓*	90.60	82.91	6.13	1.88
				✓	90.84	83.32	5.89	1.85
		✓	✓		90.77	83.20	8.27	2.50
		✓	✓*		90.63	83.03	5.99	1.61
		✓		✓	91.07	83.67	5.84	1.67
80 (100%)	0				92.05	85.33	7.10	1.79

* The consistency constraints are enforced for $p^*(y_{pred}^*|x; \theta_{sub})$ of different sub-models.

for probability outputs or soft pseudo labels, labeled by *CC* or *CC**. We also provide the fully supervised MC-Net+ model, *i.e.*, without L_{mc} for training, as the reference. The results show that simply adopting three slightly different decoders does not bring impressive performance gains while enforcing our novel mutual consistency constraints can significantly improve the semi-supervised segmentation performance with overall dice gains of 6.25% and 5.07% on the LA dataset, respectively.

6.2. Effects of Different Up-sampling Strategies

To increase the intra-model diversity, our MC-Net+ model adopts the transposed convolutional layer, the linear interpolation layer, and the nearest interpolation layer to construct three slightly different decoders. Fig. 6 indicates

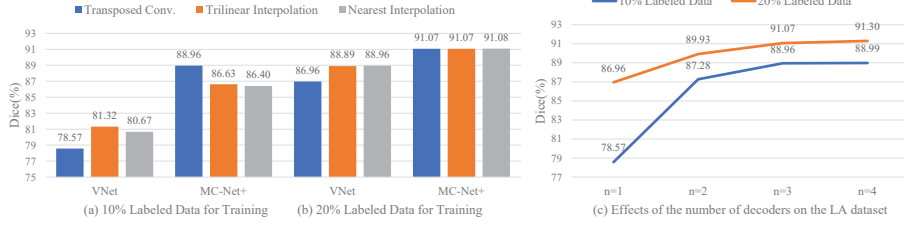


Figure 6: Dice performance of different up-sampling strategies (*a and b*) and the number of decoders (*c*) on the LA dataset. Note that, to construct four decoders, we use two transposed convolutional layers with different initialization parameters for training due to the limitation of public available up-sampling strategies.

that, the dice values of fully supervised VNet models with different up-sampling strategies vary significantly on the LA dataset. However, when applying our mutual consistency constraints, our MC-Net+ model obtains better results and three slightly decoders tend to generate invariant outputs, leading to fewer ambiguous predictions and lower model uncertainty. Since three decoders can generate similar results, we only select the original encoder-decoder architecture, *i.e.*, the shared encoder and the first decoder, as the final testing model to reduce the inference costs. Note that, our previous MC-Net model (Wu et al., 2021) employs the mean results of two decoders as final predictions while the new MC-Net+ model just uses the first outputs as final results in the experiments.

Furthermore, since the number n of decoders is scalable, we further conduct a sensitivity experiment to show the effects of n . Fig. 6 (c) shows that introducing more decoders can improve the performance, but the gains are decreased due to the confirmation biases (Li et al., 2020a). In other words, since the labeled data is extremely limited, deep models may generate wrong predictions but with high confidence. Therefore, n is set as 3 in this paper to achieve a balance between effectiveness and efficiency. We also believe that if the labeled data is adequate, our model with more diverse sub-models could obtain better performance.

6.3. Effects of Temperature T

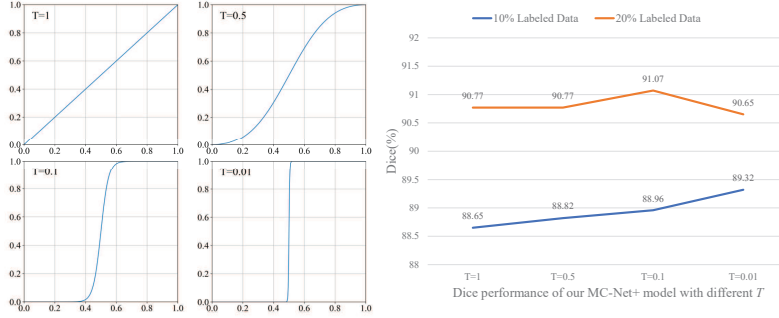


Figure 7: Illustrations of corresponding sharpening functions (*left*) and dice performance (*right*) with different sharpening temperatures T on the LA dataset.

To mitigate the effects of the easily mis-classified pixels, the MC-Net+ model uses the soft pseudo labels to apply the low-entropy constraints and does not significantly sharpen the plausible predictions around probability 0.5 (see the (*left*) of Fig. 7). Fig. 7 (*right*) gives the dice performance of our MC-Net+ model trained with different temperatures T on the LA dataset. It shows that, in each semi-supervised setting, the dice values of different T are similar, which indicates that our model is relatively robust about the hyper-parameter T . Here, a larger T cannot enforce sufficient entropy-minimization constraints for the model training while a smaller T may increase the noises, leading to the error acclimation. Therefore, for simplicity, we finally adopt the sharpening function with temperature 0.1 to generate soft pseudo labels on all datasets.

6.4. Effects of Loss Weight λ

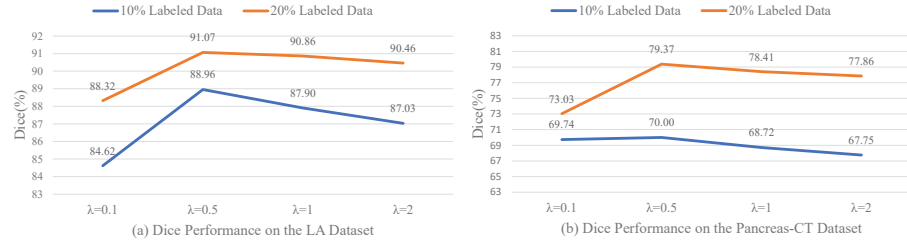


Figure 8: Dice performance with different loss weights λ on the LA (*a*) and Pancreas-CT (*b*) datasets.

We conducted a parameter sensitivity experiment on the LA and Pancreas-CT datasets, to show effects of λ for the balance between the supervised loss and the mutual consistency loss (see Fig. 8). Here, a smaller λ would decrease the performance since three decoders may generate inaccurate results due to the insufficient labeled training, while a larger λ will not apply enough mutual consistency constraints and thus also obtain a sub-optimal performance. Therefore, in this paper, we set the weight λ as 0.5 to balance two losses on all datasets.

6.5. Effects of Different Distance Measurements D

Table 5: Discussion of different distance measurements D on the LA dataset.

Method	Output	# Scans used		Metrics			
		Labeled	Unlabeled	Dice(%) \uparrow	Jaccard(%) \uparrow	95HD(voxel) \downarrow	ASD(voxel) \downarrow
MC-Net+ w/ KL	First Decoder	8 (10%)	72 (90%)	87.86	78.86	9.65	2.27
	Mean			88.04	79.08	9.40	2.32
MC-Net+ w/ MSE	First Decoder	8 (10%)	72 (90%)	88.96	80.25	7.93	1.86
	Mean			88.94	80.22	8.02	1.83
MC-Net+ w/ KL	First Decoder	16 (20%)	64 (80%)	90.93	83.45	6.04	1.63
	Mean			90.96	83.50	6.08	1.60
MC-Net+ w/ MSE	First Decoder	16 (20%)	64 (80%)	91.07	83.67	5.84	1.67
	Mean			91.08	83.70	5.90	1.60

We further discuss the effects of using different D to measure the discrepancy on the LA dataset. In Table 5, we give the results of our MC-Net+ model using the Kullback-Leibler (KL) divergence for training. We can see that the KL loss also can improve the segmentation performance in each semi-supervised setting. Nevertheless, the simple MSE loss is sufficient to demonstrate the effectiveness of our model. Therefore, we finally adopt the MSE loss as D in this paper.

6.6. Limitations and Future Work

Although our model is simple and powerful for semi-supervised medical image segmentation, the model design still requires multiple pre-defined decoders, and the selection of existing up-sampling strategies is limited. For new tasks, more varied architectures are worthwhile to be further explored to increase the intra-model diversity. Meanwhile, in this paper, we only discuss the model-level

perturbations, *i.e.*, using different up-sampling strategies, while the data-level perturbations should be also useful. However, some data-agnostic operations like ColorJitter (Sohn et al., 2020) may not be suitable for medical data. Future work will focus on developing the medical data-specific perturbation operations and using larger medical dataset to evaluate the proposed model.

7. Conclusion

In this paper, we have presented a novel MC-Net+ model for semi-supervised medical image segmentation. Effectively leveraging the challenging regions plays an important role in the semi-supervised segmentation. The model design with three slightly different decoders is used to indicate highly uncertain areas and the new mutual consistency constraint between the probability outputs and soft pseudo labels establishes an ‘end-to-end’ way to force model generate invariant predictions, especially at hard regions. Extension experiments demonstrate our model has achieved superior performance over five existing models on three medical datasets and the proposed MC-Net+ model sets a new state-of-the-art performance for the semi-supervised medical image segmentation task.

8. Acknowledgments

This work was supported by the Monash FIT Start-up Grant. We also appreciate the efforts devoted to collect and share the datasets (Xiong et al., 2021; Clark et al., 2013; Bernard et al., 2018) and several public benchmarks (Yu et al., 2019; Li et al., 2020b; Luo et al., 2021a,b; Luo, 2020).

References

Abdar, M., Pourpanah, F., Hussain, S., Rezazadegan, D., Liu, L., Ghavamzadeh, M., Fieguth, P., Cao, X., Khosravi, A., Acharya, U.R., et al., 2021. A review of uncertainty quantification in deep learning: Techniques, applications and challenges. *Information Fusion* .

- Bernard, O., Lalande, A., Zotti, C., Cervenansky, F., Yang, X., Heng, P.A., Cetin, I., Lekadir, K., Camara, O., Ballester, M.A.G., et al., 2018. Deep learning techniques for automatic mri cardiac multi-structures segmentation and diagnosis: Is the problem solved? *IEEE transactions on medical imaging* 37, 2514–2525.
- Castillo-Navarro, J., Le Saux, B., Boulch, A., Lefèvre, S., 2020. On auxiliary losses for semi-supervised semantic segmentation, in: *Proceedings of the European Conference on Machine Learning and Principles and Practice of Knowledge Discovery in Databases*, pp. 1–10.
- Chaitanya, K., Erdil, E., Karani, N., Konukoglu, E., 2020. Contrastive learning of global and local features for medical image segmentation with limited annotations. *Advances in Neural Information Processing Systems* 33, 12546–12558.
- Chen, X., Yuan, Y., Zeng, G., Wang, J., 2021. Semi-supervised semantic segmentation with cross pseudo supervision, in: *Proceedings of the IEEE/CVF Conference on Computer Vision and Pattern Recognition*, pp. 2613–2622.
- Clark, K., Vendt, B., Smith, K., Freymann, J., Kirby, J., Koppel, P., Moore, S., Phillips, S., Maffitt, D., Pringle, M., et al., 2013. The cancer imaging archive (tcia): maintaining and operating a public information repository. *Journal of digital imaging* 26, 1045–1057.
- Esser, P., Sutter, E., Ommer, B., 2018. A variational u-net for conditional appearance and shape generation, in: *Proceedings of the IEEE Conference on Computer Vision and Pattern Recognition*, pp. 8857–8866.
- Gal, Y., Ghahramani, Z., 2016. Dropout as a bayesian approximation: Representing model uncertainty in deep learning, in: *international conference on machine learning*, PMLR. pp. 1050–1059.
- Jin, L., Lu, H., Wen, G., 2019. Fast uncertainty quantification of reservoir simulation with variational u-net. *arXiv preprint arXiv:1907.00718*.

- Jungo, A., Reyes, M., 2019. Assessing reliability and challenges of uncertainty estimations for medical image segmentation, in: International Conference on Medical Image Computing and Computer-Assisted Intervention, Springer. pp. 48–56.
- Kalluri, T., Varma, G., Chandraker, M., Jawahar, C., 2019. Universal semi-supervised semantic segmentation, in: Proceedings of the IEEE/CVF International Conference on Computer Vision, pp. 5259–5270.
- Kendall, A., Gal, Y., 2017. What uncertainties do we need in bayesian deep learning for computer vision? arXiv preprint arXiv:1703.04977 .
- Laine, S., Aila, T., 2016. Temporal ensembling for semi-supervised learning. arXiv preprint arXiv:1610.02242 .
- Lakshminarayanan, B., Pritzel, A., Blundell, C., 2016. Simple and scalable predictive uncertainty estimation using deep ensembles. arXiv preprint arXiv:1612.01474 .
- Lee, D.H., et al., 2013. Pseudo-label: The simple and efficient semi-supervised learning method for deep neural networks, in: Workshop on challenges in representation learning, ICML, p. 896.
- Li, J., Socher, R., Hoi, S.C., 2020a. Dividemix: Learning with noisy labels as semi-supervised learning. arXiv preprint arXiv:2002.07394 .
- Li, S., Zhang, C., He, X., 2020b. Shape-aware semi-supervised 3d semantic segmentation for medical images, in: International Conference on Medical Image Computing and Computer-Assisted Intervention, Springer. pp. 552–561.
- Luo, X., 2020. SSL4MIS. <https://github.com/HiLab-git/SSL4MIS>.
- Luo, X., Chen, J., Song, T., Wang, G., 2021a. Semi-supervised medical image segmentation through dual-task consistency, in: Proceedings of the AAAI Conference on Artificial Intelligence, pp. 8801–8809.

- Luo, X., Liao, W., Chen, J., Song, T., Chen, Y., Zhang, S., Chen, N., Wang, G., Zhang, S., 2021b. Efficient semi-supervised gross target volume of nasopharyngeal carcinoma segmentation via uncertainty rectified pyramid consistency, in: International Conference on Medical Image Computing and Computer-Assisted Intervention, Springer. pp. 318–329.
- Ma, J., Wei, Z., Zhang, Y., Wang, Y., Lv, R., Zhu, C., Gaoxiang, C., Liu, J., Peng, C., Wang, L., et al., 2020. How distance transform maps boost segmentation cnns: an empirical study, in: Medical Imaging with Deep Learning, PMLR. pp. 479–492.
- Masood, S., Sharif, M., Masood, A., Yasmin, M., Raza, M., 2015. A survey on medical image segmentation. *Current Medical Imaging* 11, 3–14.
- Milletari, F., Navab, N., Ahmadi, S.A., 2016. V-net: Fully convolutional neural networks for volumetric medical image segmentation, in: 2016 fourth international conference on 3D vision (3DV), IEEE. pp. 565–571.
- Mittal, S., Tatarchenko, M., Brox, T., 2019. Semi-supervised semantic segmentation with high-and low-level consistency. *IEEE transactions on pattern analysis and machine intelligence* .
- Miyato, T., Maeda, S.i., Koyama, M., Ishii, S., 2018. Virtual adversarial training: a regularization method for supervised and semi-supervised learning. *IEEE transactions on pattern analysis and machine intelligence* 41, 1979–1993.
- Murugesan, B., Sarveswaran, K., Shankaranarayana, S.M., Ram, K., Joseph, J., Sivaprakasam, M., 2019. Psi-net: Shape and boundary aware joint multi-task deep network for medical image segmentation, in: Proceedings of the Annual International Conference of the IEEE Engineering in Medicine and Biology Society, IEEE. pp. 7223–7226.
- Ouali, Y., Hudelot, C., Tami, M., 2020. Semi-supervised semantic segmentation

- with cross-consistency training, in: Proceedings of the IEEE/CVF Conference on Computer Vision and Pattern Recognition, pp. 12674–12684.
- Pham, H., Dai, Z., Xie, Q., Le, Q.V., 2021. Meta pseudo labels, in: Proceedings of the IEEE/CVF Conference on Computer Vision and Pattern Recognition, pp. 11557–11568.
- Qiao, F., Peng, X., 2021. Uncertainty-guided model generalization to unseen domains, in: Proceedings of the IEEE/CVF Conference on Computer Vision and Pattern Recognition, pp. 6790–6800.
- Rizve, M.N., Duarte, K., Rawat, Y.S., Shah, M., 2021. In defense of pseudo-labeling: An uncertainty-aware pseudo-label selection framework for semi-supervised learning. arXiv preprint arXiv:2101.06329 .
- Ronneberger, O., Fischer, P., Brox, T., 2015. U-net: Convolutional networks for biomedical image segmentation, in: Proceedings of the International Conference on Medical Image Computing and Computer-Assisted Intervention, pp. 234–241. doi:[10.1007/978-3-662-54345-0_3](https://doi.org/10.1007/978-3-662-54345-0_3).
- Sohn, K., Berthelot, D., Li, C.L., Zhang, Z., Carlini, N., Cubuk, E.D., Kurakin, A., Zhang, H., Raffel, C., 2020. Fixmatch: Simplifying semi-supervised learning with consistency and confidence. arXiv preprint arXiv:2001.07685 .
- Soviany, P., Ionescu, R.T., Rota, P., Sebe, N., 2021. Curriculum learning: A survey. arXiv preprint arXiv:2101.10382 .
- Tarvainen, A., Valpola, H., 2017. Mean teachers are better role models: Weight-averaged consistency targets improve semi-supervised deep learning results. arXiv preprint arXiv:1703.01780 .
- Wang, K., Zhan, B., Zu, C., Wu, X., Zhou, J., Zhou, L., Wang, Y., 2021a. Triple-uncertainty guided mean teacher model for semi-supervised medical image segmentation, in: Proceedings of the International Conference on Medical Image Computing and Computer-Assisted Intervention, Springer. pp. 450–460.

- Wang, Y., Huang, G., Song, S., Pan, X., Xia, Y., Wu, C., 2021b. Regularizing deep networks with semantic data augmentation. *IEEE Transactions on Pattern Analysis and Machine Intelligence* .
- Wu, Y., Wu, Z., Wu, Q., Ge, Z., Cai, J., 2022. Exploring smoothness and class-separation for semi-supervised medical image segmentation. *arXiv preprint arXiv:2203.01324* .
- Wu, Y., Xu, M., Ge, Z., Cai, J., Zhang, L., 2021. Semi-supervised left atrium segmentation with mutual consistency training, in: *International Conference on Medical Image Computing and Computer-Assisted Intervention*, Springer. pp. 297–306.
- Xia, Y., Liu, F., Yang, D., Cai, J., Yu, L., Zhu, Z., Xu, D., Yuille, A., Roth, H., 2020a. 3d semi-supervised learning with uncertainty-aware multi-view co-training, in: *Proceedings of the IEEE/CVF Winter Conference on Applications of Computer Vision*, pp. 3646–3655.
- Xia, Y., Yang, D., Yu, Z., Liu, F., Cai, J., Yu, L., Zhu, Z., Xu, D., Yuille, A., Roth, H., 2020b. Uncertainty-aware multi-view co-training for semi-supervised medical image segmentation and domain adaptation. *Medical Image Analysis* 65, 101766.
- Xie, Q., Dai, Z., Hovy, E., Luong, M.T., Le, Q.V., 2019. Unsupervised data augmentation for consistency training. *arXiv preprint arXiv:1904.12848* .
- Xie, Y., Zhang, J., Liao, Z., Verjans, J., Shen, C., Xia, Y., 2020. Pairwise relation learning for semi-supervised gland segmentation, in: *International Conference on Medical Image Computing and Computer-Assisted Intervention*, Springer. pp. 417–427.
- Xiong, Z., Xia, Q., Hu, Z., Huang, N., Bian, C., Zheng, Y., Vesal, S., Ravikumar, N., Maier, A., Yang, X., et al., 2021. A global benchmark of algorithms for segmenting the left atrium from late gadolinium-enhanced cardiac magnetic resonance imaging. *Medical Image Analysis* 67, 101832.

- You, C., Zhao, R., Staib, L., Duncan, J.S., 2021a. Momentum contrastive voxel-wise representation learning for semi-supervised volumetric medical image segmentation. arXiv preprint arXiv:2105.07059 .
- You, C., Zhou, Y., Zhao, R., Staib, L., Duncan, J.S., 2021b. Simcvd: Simple contrastive voxel-wise representation distillation for semi-supervised medical image segmentation. arXiv preprint arXiv:2108.06227 .
- Yu, L., Wang, S., Li, X., Fu, C.W., Heng, P.A., 2019. Uncertainty-aware self-ensembling model for semi-supervised 3d left atrium segmentation, in: International Conference on Medical Image Computing and Computer-Assisted Intervention, Springer. pp. 605–613.
- Zhang, H., Cisse, M., Dauphin, Y.N., Lopez-Paz, D., 2017. mixup: Beyond empirical risk minimization. arXiv preprint arXiv:1710.09412 .
- Zhang, Y., Xiang, T., Hospedales, T.M., Lu, H., 2018. Deep mutual learning, in: Proceedings of the IEEE Conference on Computer Vision and Pattern Recognition, pp. 4320–4328.
- Zheng, Z., Yang, Y., 2021. Rectifying pseudo label learning via uncertainty estimation for domain adaptive semantic segmentation. International Journal of Computer Vision 129, 1106–1120.
- Zhou, Y., Li, Z., Bai, S., Wang, C., Chen, X., Han, M., Fishman, E., Yuille, A.L., 2019. Prior-aware neural network for partially-supervised multi-organ segmentation, in: Proceedings of the IEEE/CVF International Conference on Computer Vision, pp. 10672–10681.
- Zhu, J., Li, Y., Hu, Y., Ma, K., Zhou, S.K., Zheng, Y., 2020. Rubik’s cube+: A self-supervised feature learning framework for 3d medical image analysis. Medical image analysis 64, 101746.